Joint Centre for Mesoscale Meteorology, Reading, UK

Radar Estimates of Rainfall Rates at the Ground in Bright Band and Non-bright Band Events

T. J. Smyth
A. J. Illingworth

Internal Report No. 88

June 1998

Met Office Joint Centre for Mesoscale Meteorology Department of Meteorology
University of Reading PO Box 243 Reading RG6 6BB United Kingdom
Tel: +44 (0)118 931 8425 Fax: +44 (0)118 931 8791
www.metoffice.com

Designed and produced by the Met Office © Crown copyright 2001 01/0240 The Met Office logo is a registered trademark.

Radar Estimates of Rainfall Rates at the Ground in Bright Band and Non-Bright Band Events

T. J. Smyth *and A. J. Illingworth

JCMM, Department of Meteorology, University of Reading, UK

March 17, 1998

* Current affiliation: Tim Smyth, Plymouth Marine Laboratory, Prospect Place, Plymouth PL1 3DH. email: T.J.Smyth@pml.ac.uk

Abstract

The major error in estimating precipitation rates at the ground from radar arises from the change in radar reflectivity (Z) with height. In stratiform precipitation Z rises in the "bright band", where the snow is melting, and then falls steeply in the dry ice above. In regions of vigorous convection containing graupel, the bright band is absent and the fall in Z with height is less marked. If accurate estimates of surface precipitation are to be made based upon radar observations taken within or above the bright band, it is important to use a correction scheme which uses a different Vertical Profile of Reflectivity (VPR) for the two precipitation types. Using a large radar dataset, this work addresses the issue of VPR variability by constructing average vertical profiles and sorting them into snow and graupel categories using the value of the Linear Depolarisation Ratio (LDR) at the melting layer. These observations show that convection is often embedded within stratiform precipitation and some convective showers containing snow have bright bands. As a result the use of an average profile over the whole region scanned by radar leads to only marginal improvement in rain estimates. Instead, this work proposes that a bright band correction should always be applied unless the value of Z, 1.5km above the bright band height exceeds 30dBZ, in which case a "convective" vertical profile of -2dBkm^{-1} should be used. This Z threshold indicates that graupel only forms when the Ice Water Content (IWC) exceeds 0.35gm^{-3} which has implications for ice parametrisation schemes in mesoscale models.

1 Introduction

One of the major problems in using radar to estimate rainfall is that the lowest beam elevation can either overshoot the precipitation or intercept the enhanced reflectivity associated with melting snow (the "bright band"). Joss and Waldvogel (1990) stated that the major source of error in rainfall rate estimation lay not in the often researched area of the Z-R relationship, but rather in the heterogeneous nature of the vertical reflectivity profile. If the beam encounters the bright band, the rain rate will be overestimated by up to a factor of 5 at S-band and C-band; if Z is within the ice region above the bright band, the surface precipitation at that pixel will be hugely underestimated.

Figure 1 shows a typical vertical reflectivity profile (VPR). Region A is populated by a mixture of ice particles and snow. Upon the onset of melting (region B), these snow flakes acquire a shell of liquid water which causes an increase in dielectric constant. As their size is retained during the early part of melting they appear to the radar to be giant raindrops, and because Z $\propto$ Diameter ^{6}, there is a dramatic increase in the reflectivity of some 7 to 13dBZ; 5.8dB due to the change in dielectric constant, the remainder to the large size of the wet snowflakes. The higher reflectivities have larger enhancements because the flakes are larger with lower densities. Fabry and Zawadski (1995) listed six effects which are in operation at the melting layer, each contributing by a greater or lesser extent to the enhancement of reflectivity. In addition to the change in dielectric constant they postulated that the increase in particle growth rate, terminal velocity, particle size distribution, particle shape and orientation could be important factors. They asserted that melting itself is not a sufficient condition to explain the shape and magnitude of the bright band. However they did not consider the large size of the wet snowflakes. Beneath the bright band (region C) the increase in hydrometeor terminal velocity causes a reduction in the returned power as the concentration of raindrops is diminished.

In regions of vigorous convection the hydrometeors are higher density graupel or soft hail and the bright band is absent, but such areas are often surrounded by more stratiform precipitation which does have a bright band. Any scheme to correct for the bright band

must be able to recognise convective cores. If the correction scheme is applied in error to such cores then the high reflectivity regions of heavy precipitation, with the potential to cause flash floods, will be suppressed. The various schemes proposed to correct for vertical profiles of reflectivity are reviewed in section 2. A polarisation parameter which can identify the bright band is introduced in section 3 and a Z threshold proposed which has the potential to distinguish between precipitation containing snow from that containing graupel. The implications of this for mesoscale cloud modelling are also discussed. A statistical analysis of vertical profiles of reflectivity with and without bright bands is presented in section 4 and a new correction scheme is proposed in section 5.

The radar data used in this paper was obtained using the S-band ($\lambda = 9.75$cm) Chilbolton radar which is situated in southern England. The radar has polarisation capability and a narrow (0.28°) beam width which allows excellent spatial resolution of precipitation events. Details on the hardware and engineering specifications of the radar can be found in Goddard *et al.* (1994).

2 Correction Schemes.

Precipitation overshoot is a problem particularly at middle to high latitudes in the winter (e.g., Harrold *et al.* (1974), Collier (1986), Joss and Waldvogel (1990)). This is due to precipitation growth beneath the beam volume. Kitchen (1997) pointed out that over most of the land area in the UK the spacing of the operational networked radars is such that the lowest radar beam is centred more than 1km above sea level and for 5% of the area the beam centre is more than 3km altitude. The freezing level is commonly below 1km in winter (see Collier (1976) for a climatology) so, for complete radar coverage to be meaningful in terms of rainfall rate estimation, a correction to the overshooting beams (and the bright band) is needed.

Several schemes have been advanced to solve this problem operationally. Collier *et al.* (1983) proposed the use of telemetering rain gauges; this approach yielded, on average, an improvement but was limited by the inherent lack of representivity provided by a limited number

of rain gauges. Divjak (1994) used vertical profiles to correct for rainfall rate estimation in Italy. One of the problems that he encountered was the horizontal inhomogeneity of the precipitation. He calculated representative reflectivity profiles averaged over an area from 5 to 60km around the radar and over a period of one hour. This representative profile was then divided into one of two classes: stratiform if the average Z gradient above the freezing level was above -2.5dBkm^{-1} , convective if it was less. The scheme resulted in a reduction of the overall spread of radar-to-raingauge ratios from a factor of 2.6 to 2.3. The disadvantage of this method is that the same profile is applied to the whole radar scan, even when (as is usually the case) the convective cells are embedded in stratiform precipitation. Andrieu and Creutin (1995) and Andrieu *et al.* (1995) propose a correction scheme for vertical profiles through an inverse solution applied to radar data from at least two elevation angles, but this technique still relies on the strong assumption of spatial homogeneity of the vertical profile.

One problem with using a vertical profile to correct for range is determining the representivity of the profile and its associated systematic and stochastic errors (Joss and Waldvogel, 1989) . Joss and Pittini (1991) extracted average vertical profiles every 10 minutes for a grid box of size 2x10^{4}km^2. Comparing the radar estimates with rain gauges the difference in daily totals was reduced from a factor of 3 difference to a factor of 1.2. They found that even the use of climatological profiles improved the estimate of rainfall

Kitchen *et al.* (1994) describe an operational scheme for vertical profile correction using a detailed profile (Illingworth, 1991) in which the bright band enhancement is a function of reflectivity in the rain below and has been derived from high resolution (0.28° beamwidth) data taken with the Chilbolton radar. This profile (figure 2) has a constant value of Z (Zb) in the rainfall; the bright band (BB) enhancement of Z is represented by a triangular profile of depth 700m and is related to Zb. Finally, the profile in the ice is fixed using the height of the top of the echo. The correction is performed by first normalising the height of the profile so that the top of the BB coincides with the 0°C isotherm derived from an operational forecasting model. The second step in the correction is to scale the Z values of the profile so that the observed value of Z from the lowest elevation radar beam agrees

with the value obtained by multiplying the profile by the beam pattern of the radar at that range. Validation in stratiform rainfall showed a significant improvement in rainfall estimates.

The next step in improving the corrections would appear to be to use higher elevation radar beams to provide a more accurate estimate of the Z gradient rather than using a climatological profile. However, when this was done (Kitchen, 1997) no further improvement could be detected in frontal rainfall, thus confirming the assertion of Fabry *et al.* (1992) that beyond the range where the radar horizon intercepts the freezing level, "any attempt to obtain quantitative rainfall estimates is futile." It is interesting to note that for this very reason quantitative use of radar estimates of rainfall have often been limited to a range of 75km.

An alternative approach is to compute the expected vertical profile of reflectivity from a detailed microphysical model of the melting snow (Hardaker *et al.*, 1995) . The advantage would be that the appropriate profile can be computed using parameters such as lapse rate and humidity profile at a particular time and place derived from an operational mesoscale model. Our experience is that the computed profile is very sensitive to detailed assumptions of the melting process for snowflakes such as the size of the wet core of the melting snowflake; a small error in this size has an enormous effect on the predicted reflectivity but the mesoscale model provides little guidance. Accordingly, it seems that the most accurate approach is to use the statistical variation of an observed large data set of profiles for various different conditions.

Allusion has already been made to the difference in vertical reflectivity between snow and graupel showers. Many authorities (e.g., Collier *et al.* (1983), Divjak (1994), Fabry and Zawadski (1995)) seek to discriminate between different types of precipitation for use in correction algorithms. In this paper distinction will be made between precipitation containing snow and that containing graupel.

3 Discrimination Between Snow and Graupel

The linear depolarisation ratio, LDR , is an excellent discriminator between melting graupel and melting snow. LDR is defined as

$$LDR = 10log_{10}\frac{Z_{VH}}{Z_{HH}}(dB) \tag{1}$$

where Z_{HH} is the reflectivity both transmitted and received in the horizontal polarisation and Z_{VH} measures the depolarisation from the vertically transmitted signal into the horizontal. LDR senses oblate particle fall mode; values of LDR above the antenna limit of -32dB occur for particles which cant or tumble as they fall. Because water has a higher dielectric constant than dry ice, oblate wet particles have higher values of LDR .

In the UK most convective showers have bright bands accompanied by LDR values of about -16dB (Frost *et al.*, 1991) , suggesting the presence of snow. In more vigorous showers there is no discernible bright band in Z, and LDR values at the melting layer are typically -25dB, indicative of graupel. These values are theoretically consistent (figures 1 and 2 in Frost *et al.*) with both types of ice tumbling randomly, but with wet snowflakes having an average axial ratio of about 0.5 to 0.6 whereas that of graupel pellets was about 0.8. Frost *et al.* later verified these shapes by using simultaneous aircraft flights. Table 1 shows the values of LDR used in this paper to discriminate between snow and graupel showers. It is possible for moderate to intense showers to contain both snow and graupel, the latter occurring within the updraught of the storm where riming rates are greatest and the former in the more stable regions of the cloud. LDR allows the small scale distribution of the hydrometeors to be observed.

To study the difference in vertical profiles from graupel and snow the data points were extracted from vertical scans (RHIs) taken by the Chilbolton radar by splitting each scan into 3 gate (900m) range "bins". For each bin the average reflectivity at various heights and LDR values at the melting layer were recorded. Averaging was done to allow for wind shear displacing the falling hydrometeors from a vertical path. Only data between 0 and 80km from the antenna was used as beam width spread leads to a loss in resolution at longer

ranges. Figure 3 *a)* refers to a case study of 5 July 1991 when a line of severe convection embedded within stratiform rain, approached Chilbolton from the south having its origins over the continent. The data set consists of 70 RHIs spread over a three hour period. Figure 3 *b)* shows a random set for days with showery conditions covering 20 days and 38 separate RHIs. Data points to the right of the dashed line in figure 3 are indicative of snow. It shows convincingly that the 30dBZ threshold 1.3km above the bright band is rarely exceeded in snow.

The 30dBZ threshold 1.3km above the melting layer in snow corresponds to a temperature of around -5°C assuming a saturated adiabatic lapse rate (-5 → -7 °C km^{-1}). This temperature could be significant for two reasons. Firstly, -5°C is the temperature threshold which marks the acceleration in the rate of snowflake aggregation. This is due to adhesion between two colliding particles being increasingly likely above -5°C (Wallace and Hobbs, 1977) . Put simply they become "stickier". Fabry and Zawadski (1995) also observed that 1.2km above the bright band top there was a considerable increase in Z. They attributed this to an increase in the magnitude of aggregation efficiency. Secondly, -5°C marks the peak in the efficiency of the Hallet Mossop ice multiplication process (Hallet and Mossop, 1974) . Secondary ice splinters are produced as internal stresses break up frozen hydrometeors. Stewart *et al.* (1984) using probe measurements aboard an aircraft, found that the largest concentrations of ice crystals occurred at -5°C . An increase in aggregation efficiency combined with an increase in the population of ice crystals will act to raise the value of the reflectivity, although the latter will contribute very little directly. A more important effect could be that more ice crystals will be made available for the aggregation process.

Graupel showers tend to have values of Z greater than 30dBZ at this altitude. This is because graupel forms in the most vigorous sections of convection. Graupel is formed by riming, a process which requires an updraught if frozen hydrometeors, such as a snowflake, are to encounter the necessary supercooled liquid water which freezes on impact. The most vigorous convective cells have a large updraught so that liquid water content (LWC) is high enough for graupel to form.

The Z threshold above the snow melting layer has important implications for modelling micro-physical processes such as aggregation, which is poorly understood and hence difficult to parametrise. The important governing factors in the aggregation process are the concentrations, sizes and densities of the ice particles. Using a combination of radar and coincidental aircraft micro-physical measurements (Thomason *et al.*, 1995) it is possible to derive the size spectra and densities of the ice particles in a cloud and also infer possible growth processes. Once the density is known, a general relationship for IWC = f(Z) can be empirically derived. This is found to be (Thomason *pers comm*):

$$IWC = 0.042Z^{0.31} \tag{2}$$

where Z is in mm^6m^{-3} . Using 2, the Z threshold 1.3km above the melting layer corresponds to an IWC of $0.35gm^{-3}$. This IWC threshold value could prove a useful diagnostic for validating mesoscale cloud models which now carry prognostic variables for the mixing ratio of different forms of ice such as snow and graupel. Some of these models may produce too much or too little graupel which will in turn effect the precipitation rate and the LWC within the cloud. An example is given by Swann (1998) who used radiosonde data to initialise a cloud resolving model and allowed convection to occur by warming the surface slightly. By comparing the model output with radar measurements made by the Chilbolton radar, the partitioning between the hydrometeors could be validated. Days were studied where either graupel or snow showers were detected by the radar (this being apparent by the return in LDR) and a corresponding radiosonde ascent used to initialise the model. As an experiment, the equation producing graupel by riming LWC was only switched on when the IWC exceeded the threshold of $0.35gm^{-3}$. Without the threshold the model produces graupel when none was observed (see Swann (1998) for detailed results). The threshold has the effect of prescribing the value of snow mass concentration before snowflakes are converted to graupel via the process of riming liquid cloud (liquid water). These results show that more realistic modelling of clouds can be made using the IWC threshold for riming.

4 Analysis of VPRs.

Vertical (Range Height Indicator or RHI) scans from the Chilbolton data set were selected where both coincidental Z_H and LDR were recorded. The value of Z was sampled at prescribed heights relative to the melting layer and a complete vertical profile constructed for every 300m range gate between 0 and 80km from the radar. The small spatial scale was used to enable resolution of the high reflectivity cores. The height of the melting layer for moderate showers and stratiform precipitation was fixed for each separate range gate profile as the height where LDR was a maximum. This value was also used to characterise the vertical profile in terms of snow or graupel. The discrimination limits used are those shown in table 1. Using this method to fix the melting layer height in severe convection is more problematic. Wet hail, forming at altitudes far above the melting layer, can give LDR returns typical of melting graupel or even snow and result in spurious fixing of the melting layer height. Therefore for the three days of severe convection studied the melting layer height is not fixed automatically using the altitude of the maximum LDR return at each range gate profile. Rather it is fixed for the whole scan using the peak in the histogram of the height where LDR associated with melting graupel (or melting snow) is found. Once the LDR and Z data have been collected for each scan the vertical profiles are categorised in terms of the reflectivity 500m below the melting layer. The value of Z at this altitude is taken to be representative of the reflectivity in the rain (Divjak, 1994) . The various profiles are sorted in their entirety into 5dBZ interval "rain bins" between 0 and 65dBZ.

a) Stratiform.

Data was collected from 5 days of stratiform precipitation consisting of 72 RHIs and 7892 vertical profiles. Stratiform precipitation was defined as having values of LDR $\geq$ -18dB (Frost *et al.*, 1991) over a widespread region of the scan. Each RHI is separated by at least 4 minutes from any other in the dataset. The results are presented to act as a comparison with the convective precipitation and to lead to better formulation of bright band removal algorithms when convection is active. Figure 4 shows the median reflectivity profiles for the data collected; the reflectivity is considered to be constant from 500m below the bright band

to the ground. Several qualitative observations can be made. Firstly the profiles contain snow above the melting layer, deduced from the values of LDR . This is hardly surprising as stratiform precipitation is characterised by gentle uplift of the order of a few cm s^{-1} rather than the more vigorous ascent experienced in severe convection; the rapid riming of snow which leads to graupel formation requires high vertical velocities. Secondly as Z increases in the rain there is a corresponding increase in the reflectivity slope above the bright band. Fabry and Zawadski (1995) attributed this increased gradient with height above the freezing level to the increasing importance of aggregation compared to the mechanisms of accretion and deposition of water vapour. The latter two mechanisms are important at lower rain reflectivities (0 - 10dBZ). Figure 5 shows the standard deviations associated with the median reflectivity profiles for the 30 - 35dBZ, 35 - 40dBZ and 40 - 45dBZ rain bins. These are the important profiles as they represent surface rainfall rates greater than 2.7mmhr ^{1} and up to 23.7mmhr^{-1} . The standard deviations are quite large and overlap considerably, especially at greater altitudes. This is shown clearly in table 2. For example the standard deviation at 1.5km above the melting layer for the 30 - 35dBZ rain bin is $\pm$5dBZ, which is a factor of $\pm$2 in terms of rainfall rate estimation. The overlap between the vertical profiles in terms of rainfall rate estimation at first sight would seem to preclude them for use in surface rainfall estimates. (It is unlikely that averaging over a greater number of gates, which would in effect simulate the radar response at a lower resolution, will reduce this noise.) This would be consistent with the results of Kitchen (1997) where no marked improvement was found by applying an idealised vertical profile above the bright band. The variability is too great at increasing altitude to allow the surface rainfall to be extracted and a fixed value of Z at a certain height can diverge to several solutions. This can be shown by using figure 5 to make a few example calculations. Taking a reflectivity of 12dBZ at a height of 3km above the melting layer (Z_{3km}) could feasibly result in the use of 3 median reflectivity profiles, namely the 30 - 35dBZ, 35 - 40dBZ and 40 - 45dBZ rain bins with their associated standard deviations at the surface. If the "ground truth" reflectivity (Z_b) is assumed to be 37dBZ then comparisons can be made with Z_{3km} and associated errors. To convert the value of Z

into a rainfall rate equation 3 will be used.

$$Z - 200R^{1.6} \tag{3}$$

Z_b and Z_{3km} are equivalent to rainfall rates of 8.0mmhr^{-1} and 0.2mmhr^{-1} respectively. In other words the beam overshooting the precipitation to a height of 3km above the melting layer will underestimate the rainfall rate by a factor of 40. If the vertical profiles were used to adjust for the precipitation overshoot this error could be considerably reduced. The surface value of Z (Z_b) given a value of Z_{3km} of 12dBZ, would lie between 30 and 45dBZ. This results in equivalent rainfall rates of 2.7mmhr^{-1} and 23.6mmhr^{-1} respectively. The error in the rainfall rate estimation would be reduced therefore from an underestimate by a factor of 40 to an under/overestimate by a factor of ± 3. This is still a considerable error when compared with the errors of about 40% associated with using a particular Z-R relationship (Goddard and Cherry, 1984) . There is also an important additional problem of the beam spreading at greater ranges. For example if the beam width is 1° (a typical value) the beam will have spread to a depth of 1km at a range of 60km. This is twice the vertical resolution of the Z profile. The technique of multiplying a standard profile by beamwidth (Kitchen *et al.*, 1994) overcomes this.

A simpler way of extracting Z_b is to produce a polynomial fit between the value of Z at various heights relative to the melting layer and Z_b. Figure 6 shows an approximately linear relationship between the value of Z at the melting layer (Z_{melt}) with Z 500m below the melting layer height (Z_b). In figure 6 the enhancement in the melting layer is slightly underestimated as Z_{melt} was the value of Z where LDR was a maximum, this was sometimes between 100 and 200m different from the height of maximum Z. The correlation between the polynomial fit and the data of 0.91 suggests that there should be a great deal of benefit in implementing this scheme to reduce errors in rainfall rate estimation around the melting layer. Any benefit in using a polynomial fit is reduced with increasing altitude as there is a considerable increase in the amount of data spread. This is shown by the reduction in the correlation coefficient. Table 3 shows the values of the polynomial (first order) coefficients which are in the form of $\alpha_0 Z_b + \alpha_1$. At heights of 3.5 and 4km above the melting layer the correlation coefficient drops lower than 50% which stops any polynomial

being of quantifiable use. Fortunately the UK network spacing is sufficiently dense to allow most of the land surface area to be within 100km from a radar. It is therefore unusual for the lowest elevation beam to overshoot the bright band by more than 1.5km. When the beam encounters ice at this elevation it still leads to an underestimation of the rainfall rate by about a factor of three (calculated from the 35-40dBZ median profile, figure 5). However when the rainfall rate is estimated using a multiple beam method such as proposed by Kitchen (1997), then altitudes of 3.5 and 4km are frequently encountered. Consider the worst case scenario where the 0°C isotherm is 500m above the ground. The radar beam at elevation 1.5° would intersect 4km in altitude (3.5km above the melting layer) at a range of 115km. This means that data from scans at elevations greater than 1.5° at the longest ranges, especially in the winter, is frequently at an altitude where disentangling of the surface rainfall rate is futile.

b) Moderate Showers.

The dataset of convective precipitation consists of 200 RHIs with 5312 profiles spread over 23 days. Three of the days covered exceptionally intense convective outbreaks (surface reflectivities exceeded 55dBZ) and most of the data for these days will be covered in section c). Figure 7 shows a comparison between the stratiform, snow and graupel shower cases. The number of snow shower profiles is low because showers by their very nature take up a smaller area than more widespread stratiform precipitation.

Comparing the snow shower profile with that of the stratiform precipitation, shows that the snow profile is steeper than that of the stratiform at altitudes greater than 1.5km above the melting layer. (Although it must be noted that there is a severe deficit in the number of snow profiles in comparison with the stratiform.) This could be due to the increased amounts of Liquid Water Content (LWC) available in convective compared with stratiform clouds; typical values being $1.0 gm^{-3}$ and $0.1 gm^{-3}$ respectively.

The graupel vertical profile (which includes profiles from the severe convection cases detailed in *c.*) is more vertically homogeneous than both the stratiform and snow cases. The pronounced bright band is absent. The increase in reflectivity caused by aggregation above

the melting layer does not occur. This is because the graupel is physically different to dendrites which adhere together when they become entwined on impact. Graupel particles would tend to rebound on impact due to their shape and density. Graupel is formed by the riming, rather than the aggregation, of ice crystals. Beneath the melting layer the reflectivity decrease is not apparent to such an extent because the terminal velocity of graupel ($2.5ms^{-1}$) is greater than that of snow ($\sim 1ms^{-1}$) and the size of wet graupel is similar to that of a raindrop. This could mean that graupel is surviving in its frozen state further beneath the bright band.

Table 4 shows that although the median profile is more vertically homogeneous than that associated with snow, there are large standard deviations associated with each data point. Part of this could be due to the small scale structure of graupel regions in a convective cell, typical dimensions being 5km in diameter. Another factor could be the growth and decay of graupel showers and their associated precipitation falling out rapidly compared with aggregates. Most of the standard deviation quoted for the graupel showers is as a result of the most vigorous convective cells. The updraughts can be so vigorous as to result in a "top heavy" reflectivity profile, in other words the reflectivity aloft is greater than that at the ground. This can be caused by hail forming in the icing regions of the cloud. Fortunately these profiles are short lived as the hail quickly descends towards the ground level by virtue of its large terminal velocity which may be of the order of $30ms^{-1}$ for large hail.

c) Severe Convection.

The dataset for the strongly convective cases was collected on three separate days. During these storms the precipitation consisted of heavy rain and hail which was reported at several locations. Figure 8 shows the contrast between strong convection and stratiform precipitation classified by LDR . The profiles categorised into the strong convection section were all found to have graupel at the melting layer using the value of LDR . As in the comparison between the stratiform and moderate showers, the bright band is absent for the showers containing graupel. The reflectivity field is very much more vertically homogeneous

than is the case for stratiform precipitation and the reflectivities are much more intense to greater altitudes. The major difference occurs above the melting layer. The stratiform profiles decrease in the magnitude of Z rapidly with height whereas in the convective cells the gradients are somewhat less. This can be seen by comparing tables 5 and 6. The stratiform first order polynomials show an increase in the negative gradient (α_0) with increasing rain rate; this is matched by a corresponding increase in the correlation between the fit and the data. The convective dataset however has a negative gradient $\sim$ -2dBZ km^{-1} for all rain rate intensities. This implies that individual gradients cannot be used to ascertain the value of Z_b in convective cases. The trend is more marked in stratiform but again the differences are so small between the relative profiles as to render any extraction of the surface rainfall rate impossible. Clearly any correction scheme would have to take account of the different vertical Z structure of graupel showers compared with stratiform precipitation and snow showers, otherwise overcorrection will occur. This will be most pronounced in severe convection.

Figure 8 shows that at altitudes over 1km above the melting layer 30dBZ is not exceeded in the stratiform precipitation. If values greater than 30dBZ are encountered above the melting layer then the convective profiles should be used to correct for precipitation overshoot.

5 Bright Band Correction Scheme

The bright band correction scheme devised by Kitchen *et al.* (1994) relies on the measurements of Z at the lowest elevation beam and the distance from the bright band to the precipitation top, H. The code iterates until the modelled profile, multiplied by the radar beamwidth, gives the observed Z. The scheme has a choice of four possible profiles depending upon the distance H. The profile scales as a background value of Z, Z_B i.e., Z in the rain. This is adjusted until Z_B gives the observed Z when the lower beam is multiplied by the profile.

An equivalent algorithm using the Chilbolton data does not require an iterative step as the beam width is very narrow (0.28°). In heavy rain the top of the precipitation is more than

4 or 5km above the bright band. Using figure 4 from Kitchen *et al.* (1994), Z in the rain (Z_b) can be approximated by subtracting 5dBZ from Z in the bright band (Z_{bb}). This is nearly equivalent to the relationship between Z_{bb} and Z_b derived from the vertical profiles in figure 8.

Both the stratiform and convective datasets collected were merged together and then used in the schemes described below. Scheme 1 is a direct implementation of the Kitchen *et al.* (1994) algorithm for a narrow beam radar and it implicitly assumes that all the profiles are stratiform in nature and that the value of Z at the melting layer height is always greater than Z_b. This is not the case for convective storms. Figure 9a) shows that the scheme needs to be modified for strongly convective cases. The data points in this region deviate significantly away from the line representing equality between the predicted and measured values of Z. Another relationship needs to be derived for strongly convective cases. A threshold value of Z=30dBZ, this time set to 1.5km above the bright band, was used to delimit between the snow and graupel profiles. This has been used in scheme 2. If the threshold is exceeded, then 1.45dBZ is added to the value of Z_{bb}. If not, then 5dBZ is subtracted from Z_{bb} as in scheme 1. The value of 1.45dBZ was obtained by finding the average value of the enhancement of Z between the melting layer height and the rain from the median profiles. Comparing figures 9 a) and b) a marked improvement is shown in the accuracy of the predicted values of Z at higher reflectivities. The correlation coefficient between the actual and predicted value of Z_b, increases from 0.94 to 0.95 upon the addition of the threshold. This could be unrepresentative of the total improvement as it is in the higher, more data sparse, values of Z where the difference is made. The improvement at higher values of Z is also shown in table 7. The figures were calculated by putting the data points into 1dBZ wide "bins" based on the actual measured value of Z_b, and the mean and standard deviation calculated for the predicted Z_b. There is no improvement at the lower values of Z_b, which is to be expected, but at values of $Z_b \geq 30$dBZ there is an increasingly marked difference between the two schemes.

Scheme 3 was developed along these lines but this time median profiles were used to predict the value of Z_b. Two lookup tables of median profiles were constructed from the datasets

of convective and stratiform precipitation. The lookup table profiles were categorised into being stratiform or convective by the value of LDR at the bright band, the convective profiles being associated with graupel and stratiform with snow. Therefore the stratiform lookup will categorise snow showers along with stratiform precipitation. A selection of the median profiles can be seen in figures 4, 5 and 8. The threshold value of Z=30dBZ, 1.5km above the melting layer, was used to decide which lookup table to use. If this threshold was exceeded then the convective median profiles were used, otherwise the stratiform profiles utilised. From an operational perspective, the height of the bright band can be fixed using the output from the mesoscale model.

Scheme 3 used the measured value of Z_{bb} to predict, via the relevant lookup table, the value of Z_b. It is a considerable improvement on scheme 1 at all but the very lowest values of Z. The improvement over scheme 2 is more marginal, most improvement being seen between 20 and 50dBZ. These values of Z are most often observed in moderate to intense rainfall, and therefore scheme 3 should be implemented in preference to the others. The correlation coefficient between the predicted and measured values of Z is 0.95. The standard deviations from each of the three schemes are all very similar as this is due to the natural variability of the profiles rather than a particular scheme's accuracy.

Both scheme 2 and 3 show the importance of being able to delimit between convective and stratiform precipitation in terms of the surface reflectivities and consequently rainfall rates. The scheme of Kitchen *et al.* (1994) would considerably underestimate the value of Z_b in the presence of strong convection; there is some evidence of this occurring in practice. This can be overcome by use of the Z=30dBZ threshold, 1.5km above the bright band, to delimit between the two precipitation types. Scheme 3 is able to distinguish between snow and graupel implicitly without the need for LDR . Within scheme 3 a convective or stratiform median vertical profile is fitted by virtue of the value of Z, 1.5km above the melting layer alone. This means that the scheme, using the LDR derived lookup tables, can be implemented operationally on radars which have no polarisation capabilities.

For an operational radar the errors may well be less than those quoted in table 7 which were

derived from profiles with a 300m gate resolution; averaging over greater distances could remove some of the small scale variability introduced, for example, by wind shear.

On the 12 August 1996 the UK networked radar situated at Chenies, situated in the Chiltern Hills to the North of London, observed a severe convective storm over Folkestone, some 120km away. The lowest beam of the radar intercepted the storm at a height where the mesoscale model was predicting that the bright band should be present. This lead the automated radar adjustment to "correct" for the high values of reflectivity ($\sim$50dBZ) that were observed, as if the precipitation was stratiform in nature (M. Kitchen *pers comm*). This lead to a considerable underestimate of the rain rate that was experienced at the surface, this being verified by cumulative raingauge totals beneath the storm.

Clearly the adjustment to the reflectivity should not have occurred in this case; a vertical profile consistent with severe convection should have been utilised instead of one designed for use in winter stratiform precipitation. The mistake could have been eliminated if Z from other elvations had been used and a vertical profile built up of the storm.

6 Conclusions

The vertical reflectivity profiles for graupel showers and particularly those in severe convection differ considerably from those found in snow showers and stratiform precipitation. A threshold in reflectivity of 30dBZ, 1.3km above the bright band, can potentially be used to delimit between snow and graupel showers. A bright band correction scheme was devised to make use of this threshold and the inherent differences between the Z profiles of snow(stratiform) and graupel(convective). The median profiles were derived using the polarisation radar data from Chilbolton but have the potential for use on any radar which uses Z alone. The precipitation was categorised into graupel or snow by the value of Z, 1.5km above the melting layer, and the value of Z in the rain predicted using an appropriate vertical profile. Schemes which were able to distinguish between precipitation containing graupel or snow gave improved estimates of the surface reflectivities, especially when $Z_b \geq 30$dBZ.

The use of two different correction profiles dependent upon the value of Z 1.5km above the bright band, appears to identify regions of embedded convection far more efficiently than the use of average profiles over a whole scan. The correction scheme proposed should reduce rainfall estimates when bright band contamination is occurring, whilst also faithfully detecting the heavy rainfall associated with graupel in convective cores. The reflectivity threshold implies that graupel is only present when the IWC exceeds 0.35gm ^{3} and could be used in mesoscale models as a constraint in formulating equations for the riming of snow and also as a model validation tool.

7 Acknowledgements

This work was supported by NERC "HYREX" grant GST/02/718.
We thank the RCRU group at RAL for allowing access to the Chilbolton radar.
Special thanks go to Malcolm Kitchen at the UK Met. Office for helpful comments and for testing the bright band removal scheme on the C-band radar network.

References

Andrieu, H. and Creutin, J. D. (1995). Identification of vertical profiles of radar reflectivities for hydrological applications using an inverse method. Part I Formulation. *J. Appl. Meteor.*, **34**, 225–239.

Andrieu, H., Delrieu, G., and Creutin, J. D. (1995). Identification of vertical profiles of radar reflectivities for hydrological applications using an inverse method. Part II Sensitivity analysis and case study. *J. Appl. Meteor.*, **34**, 240–259.

Collier, C. G. (1976). The height of the freezing level during rainfall over the British Isles. *Meteorol. Mag.*, **105**, 381–392.

Collier, C. G. (1986). Accuracy of rainfall estimates by radar, Part I: Calibration by telemetering rainguages. *J. Hydrol.*, **83**, 207–223.

Collier, C. G., Larke, P. R., and May, B. R. (1983). A weather radar correction procedure for real-time estimation of surface rainfall. *Quart. J. Roy. Meteor. Soc.*, **109**, 589–608.

Divjak, M. (1994). Radar measurement of precipitation: The use of vertical reflectivity profiles. In *Cost 75*, pages 73–84, Brussels, Belgium.

Fabry, F. and Zawadski, I. (1995). Long-term radar observations of the melting layer of precipitation and their interpretation. *J. Atmos. Sci.*, **52**, 838–851.

Fabry, R., Austin, G. L., and Tees, D. (1992). The accuracy of rainfall estimates by radar as a function of range. *Quart. J. Roy. Meteor. Soc.*, **119**, 1427-1463.

Frost, I. R., Goddard, J. W. F., and Illingworth, A. J. (1991). Hydrometeor identification using cross polar radar measurements and aircraft verification. In *25th Conference on Radar Meteorology*, pages 658–661, Paris, France. Amer. Met. Soc.

Goddard, J. W. F. and Cherry, S. M. (1984). The ability of dual polarisation radar (copolar linear) to predict rainfall rate and microwave attenuation. *Radio Sci.*, **19**, 201–208.

Goddard, J. W. F., Eastment, J. D., and Thurai, M. (1994). The Chilbolton advanced meteorological radar: a tool for multidisciplinary research. *Electronics & Communications Engineering J.*, **6**, 77–86.

Hallet, J. and Mossop, S. C. (1974). Production of secondary ice crystals during the riming process. *Nature*, **249**, 26–28.

Hardaker, P. J., Holt, A. R., and Collier, C. G. (1995). A melting layer model and its use in correcting for the bright band in single polarisation radar echoes. *Quart. J. Roy. Meteor. Soc.*, **121**, 495–525.

Harrold, T. W., English, E. J., and Nicholass, C. A. (1974). The accuracy of radar-derived rainfall measurements in hilly terrain. *Quart. J. Roy. Meteor. Soc.*, **100**, 331 350.

Illingworth, A. J. (1991). Assessment of bright band correction procedures. Meteorological Office report.

Joss, J. and Pittini, A. (1991). The climatology of vertical profiles of radar reflectivity to improve estimates of precipitation. In *25th Conference on Radar Meteorology*, pages 828–831, Paris, France. Amer. Met. Soc.

Joss, J. and Waldvogel, A. (1989). Precipitation estimates and vertical reflectivity profile corrections. In *24th Conference on Radar Meteorology*, pages 682–688, Tallahasse, Florida. Amer. Met. Soc.

Joss, J. and Waldvogel, A. (1990). *Radar in Meteorology. Ed. Atlas, D.*, chapter 29a: Precipitation, measurement and hydrology, a review, pages 577 606. AMS, Boston, 1st edition.

Kitchen, M. (1997). Towards improved radar estimates of surface precipitation. *Quart. J. Roy. Meteor. Soc.*, **123**, 145–163.

Kitchen, M., Brown, R., and Davies, A. G. (1994). Real-time correction of weather radar for the effects of bright band, range and orographic growth in widespread precipitation. *Quart. J. Roy. Meteor. Soc.*, **120**, 1231–1254.

Stewart, R. E., Marwitz, J. D., Pace, J. C., and Carbone, R. E. (1984). Characteristics through the melting layer of stratiform clouds. *J. Atmos. Sci.*, **41**, 3227–3237.

Swann, H. (1998). Sensitivity to the representation of precipitating ice in CRM simulations of deep convection. *Atmos. Research.(in press)*, **48**.

Thomason, J. W. G., Illingworth, A., and Marecal, V. (1995). Density and size distribution of aggregating snow particles inferred from coincidental aircraft and radar observations. In *27th Conference on Radar Meteorology*, pages 127–129, Vail, Colorado. Amer. Met. Soc.

Wallace, J. M. and Hobbs, P. V. (1977). *Atmospheric Science an Introductory Survey*. Academic Press.

Captions

Figure 1: Typical vertical reflectivity profile for shower containing snow. The various regions labelled are descibed in the text.

Table 1: LDR limits in Snow and Graupel.

Table 2: Standard deviations from the median at each height associated with 5dBZ wide rain bins.

Figure 2: Idealised vertical profile with approximate heights associated with each feature. (After Kitchen *et al.* (1994))

Figure 3: LDR vs Z_H at a height of 1.3km above the melting layer for *a)* 5/7/91 case study and *b)* 20 days of showery precipitation. Solid line is 30dBZ threshold and dashed line LDR = -18dB. To the right of the dashed line precipitation contains snow above the melting layer; to the left graupel.

Figure 4: Median Z profiles at height sampling intervals of 500m for 5dBZ rain intervals in stratiform precipitation.

Figure 5: Standard deviations associated with the median reflectivity profiles for the 30-35, 35-40, 40-45dBZ rain bins.

Figure 6: Linear fit between Z_{rain} and Z_{melt} for stratiform precipitation.

Table 3: Polynomial fits with associated correlation coefficients to obtain surface reflectivity from various heights.

Table 4: Standard deviations associated with each precipitation type for the 30-35dBZ rain bin median vertical profile.

Figure 7: Comparison between 30-35dBZ rain bin median vertical profile for stratiform (1092 cases), snow showers (27 cases) and graupel showers (303 cases). The frequency of snow showers exceeds that of graupel showers at lower rain-bins.

Figure 8: Contrast between severe convection (dashed) and stratiform (solid) vertical Z profiles. The graupel profile in figure 7 includes data from the severe convection cases.

Table 5: Polynomial fits for *stratiform* data points between 0.5 and 4km above the melting layer of the median vertical Z profile in each rain bin.

Table 6: Polynomial fits for *convective* data points between 0.5 and 4km above the melting layer of the median vertical Z profile in each rain bin.

Table 7: Comparison of the actual compared with the predicted Z value for 1dBZ wide "bins". See text for descriptions of schemes 1-3.

Figure 9: Predicted vs actual Z_{rain} a) Kitchen *et al.* (1994); subtracting 5dBZ from Z_{bb} b) using Z threshold 1.5km above bright band c) using median profiles and d) their associated standard deviations.

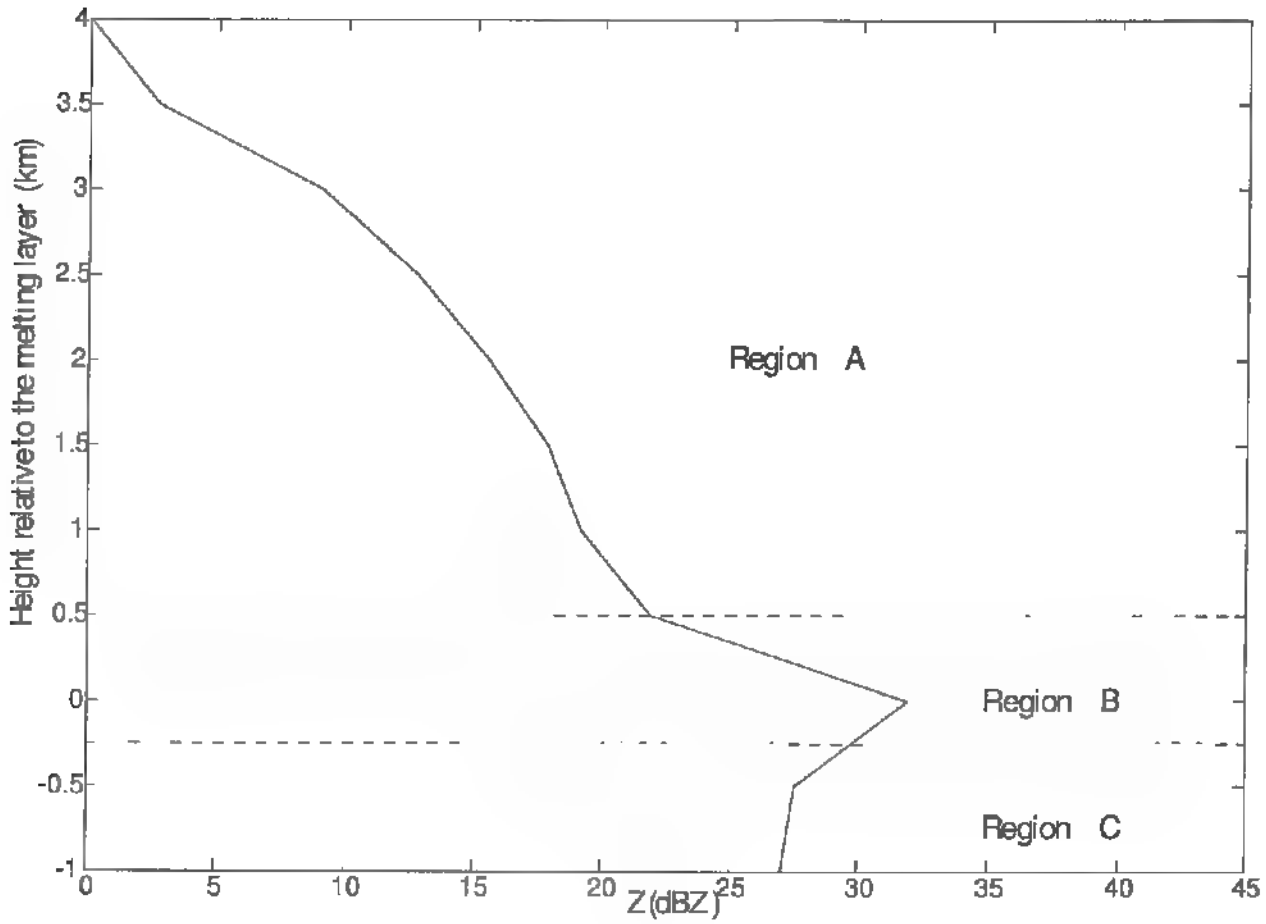
Height relativeto the melting layer (km)
Z(dBZ)
Region A
Region B
Region C
4
3.5
3
2.5
2
1.5
1
0.5
0
-0.5
-1
0
5
10
15
20
25
30
35
40
45

Figure 1:

Shower Type	LDR Limits (dB)
Graupel	-28 $\leq$ LDR $<$ -22
Snow	-18 $\leq$ LDR $<$ -12

Table 1:

Height relative to the melting layer (km)	30 - 35dBZ median $\pm$ Std	35 - 40dBZ median $\pm$ Std	40 - 45dBZ median $\pm$ Std
-0.5	32.6 $\pm$ 1.5	36.9 $\pm$ 1.3	41.2 $\pm$ 1.1
0.0	38.3 $\pm$ 3.4	42.8 $\pm$ 2.8	46.75 $\pm$ 2.4
0.5	27.4 $\pm$ 4.1	30.2 $\pm$ 3.5	32.6 $\pm$ 4.9
1.0	24.1 $\pm$ 4.1	26.1 $\pm$ 2.8	27.4 $\pm$ 3.5
1.5	22.5 $\pm$ 5.0	23.9 $\pm$ 3.5	24.5 $\pm$ 3.7
2.0	20.3 $\pm$ 6.3	21.1 $\pm$ 4.6	21.0 $\pm$ 4.9
2.5	16.2 $\pm$ 6.6	17.0 $\pm$ 5.2	15.5 $\pm$ 5.9
3.0	11.4 $\pm$ 6.4	11.2 $\pm$ 5.3	11.0 $\pm$ 5.0
3.5	8.0 $\pm$ 6.1	7.8 $\pm$ 5.5	8.1 $\pm$ 5.0
4.0	2.9 $\pm$ 5.9	4.9 $\pm$ 5.2	4.5 $\pm$ 4.2

Table 2:

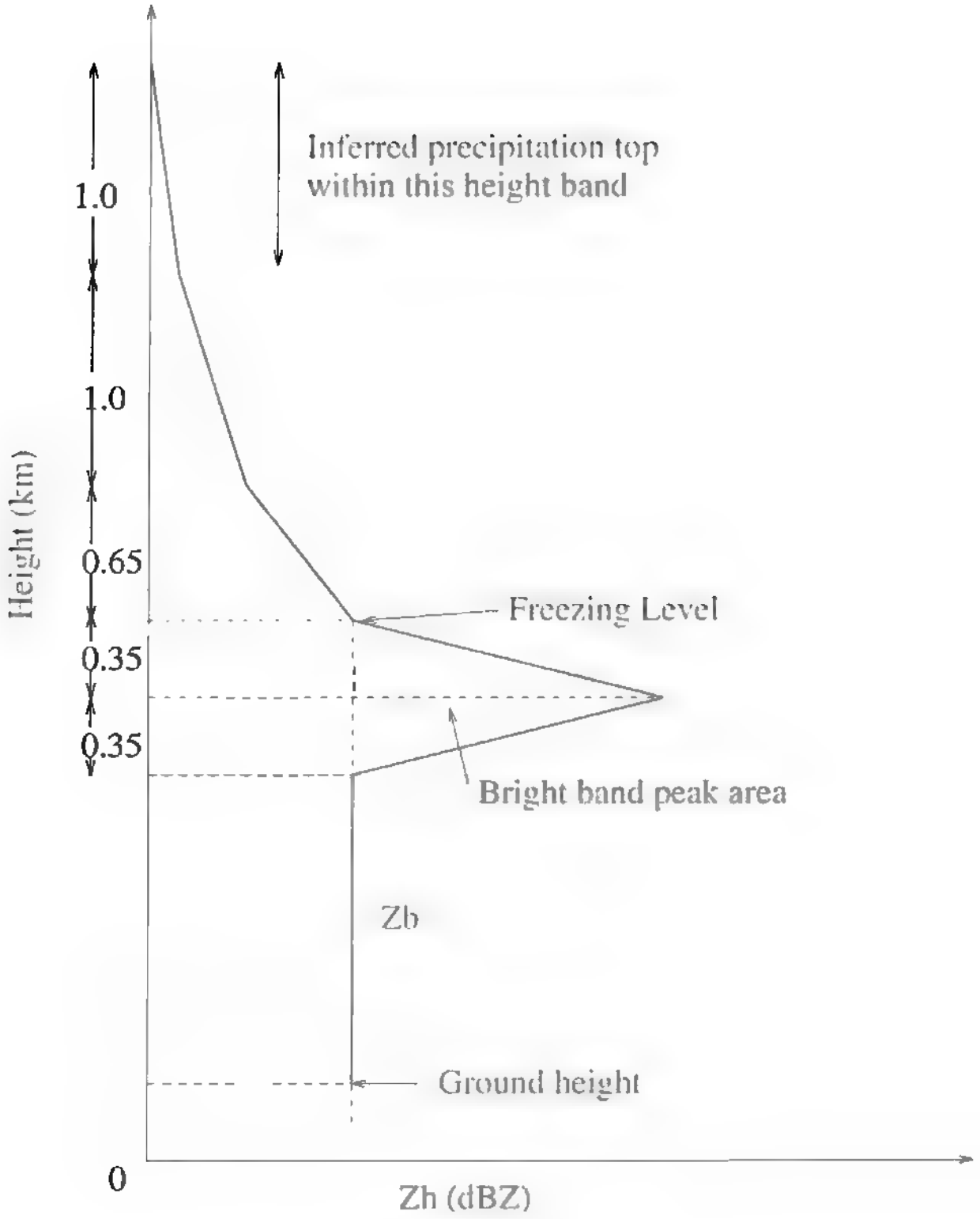
Inferred precipitation top
within this height band
1.0
1.0
0.65
0.35
0.35
Height (km)
Freezing Level
Bright band peak area
Zb
Ground height
0
Zh (dBZ)

Figure 2:

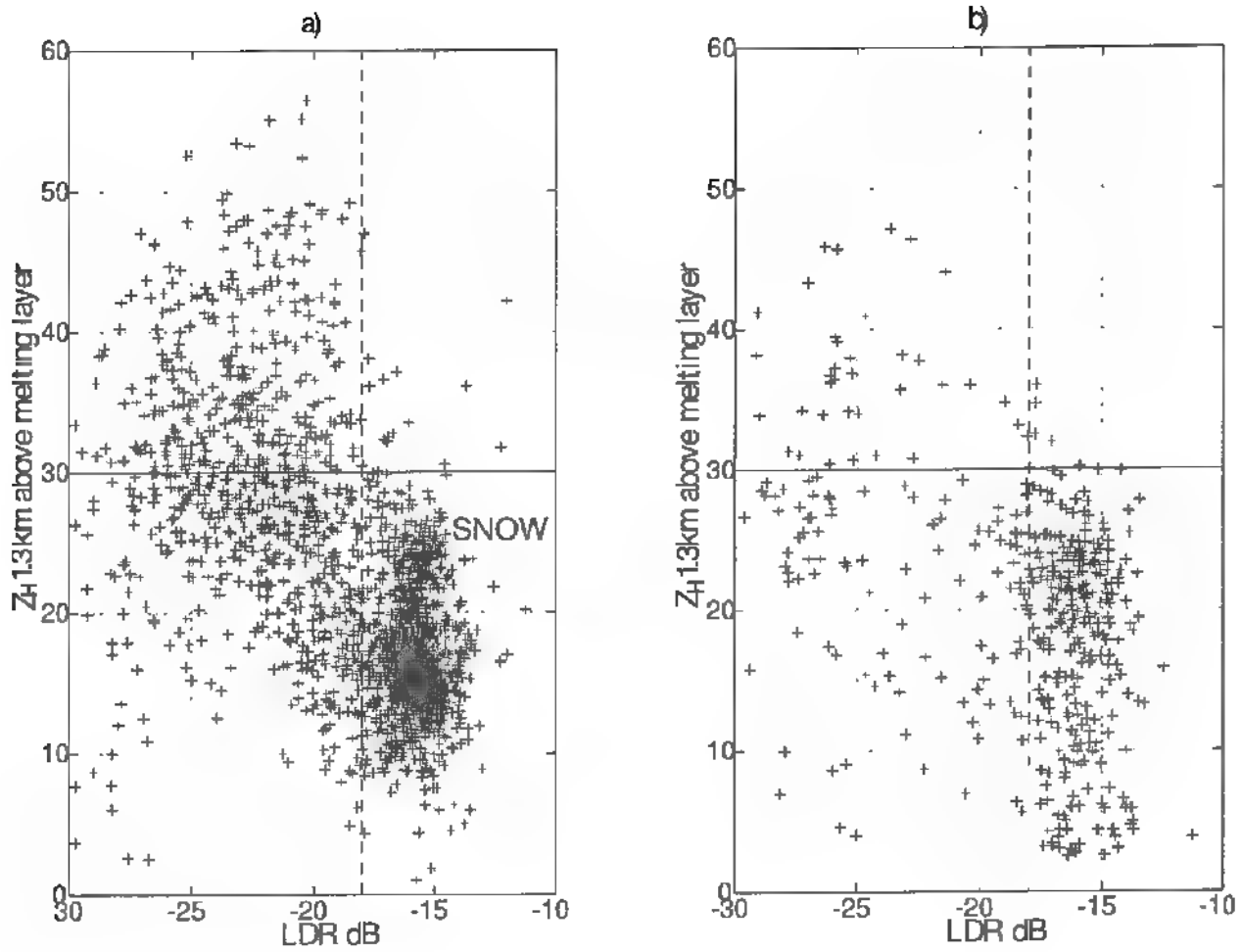
a)
b)
SNOW
Z_H 1.3km above melting layer
LDR dB
60
50
40
30
20
10
0
-30
-25
-20
-15
-10

Figure 3:

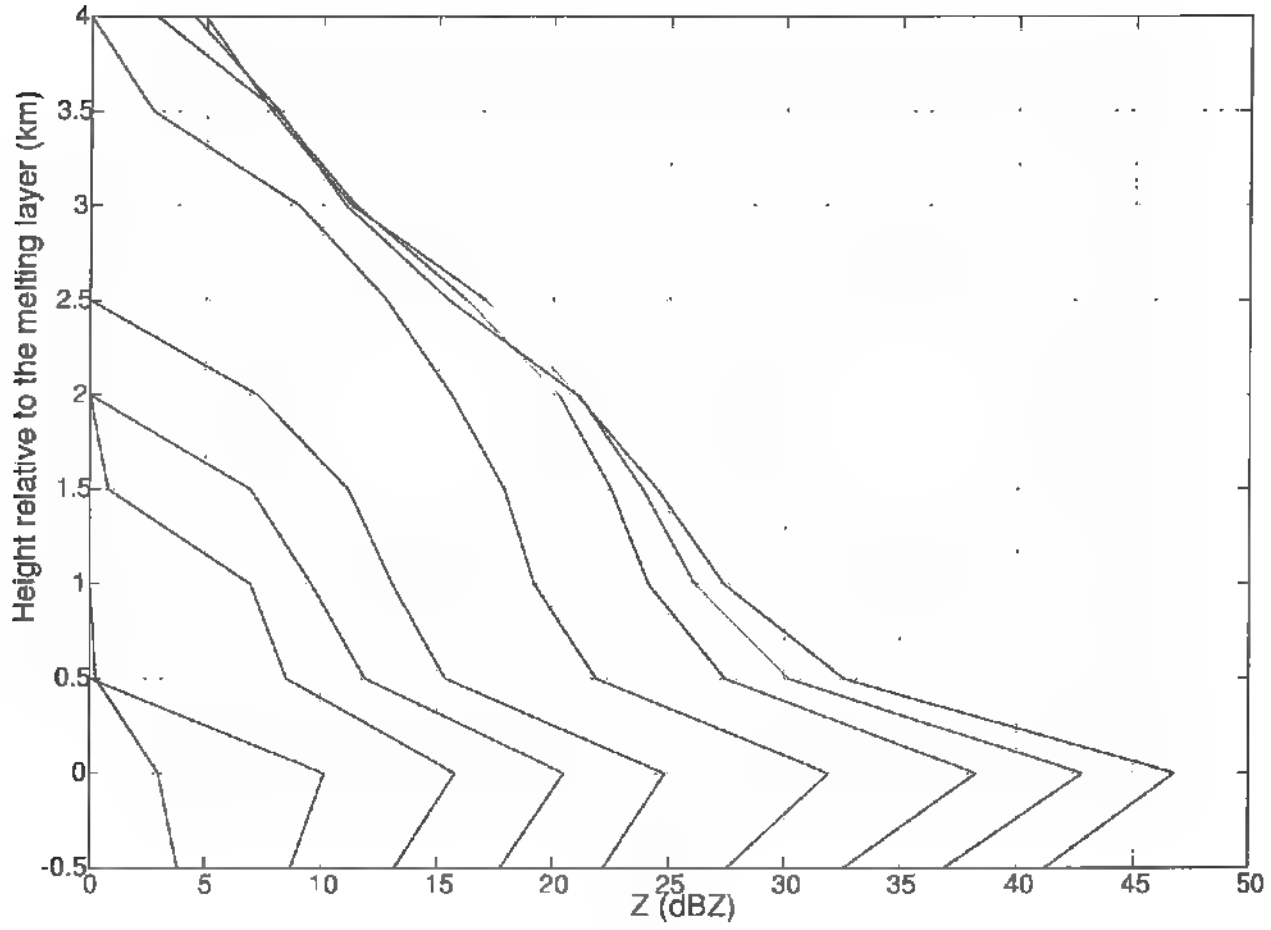
Height relative to the melting layer (km)
Z (dBZ)
4
3.5
3
2.5
2
1.5
1
0.5
0
-0.5
0
5
10
15
20
25
30
35
40
45
50

Figure 4:

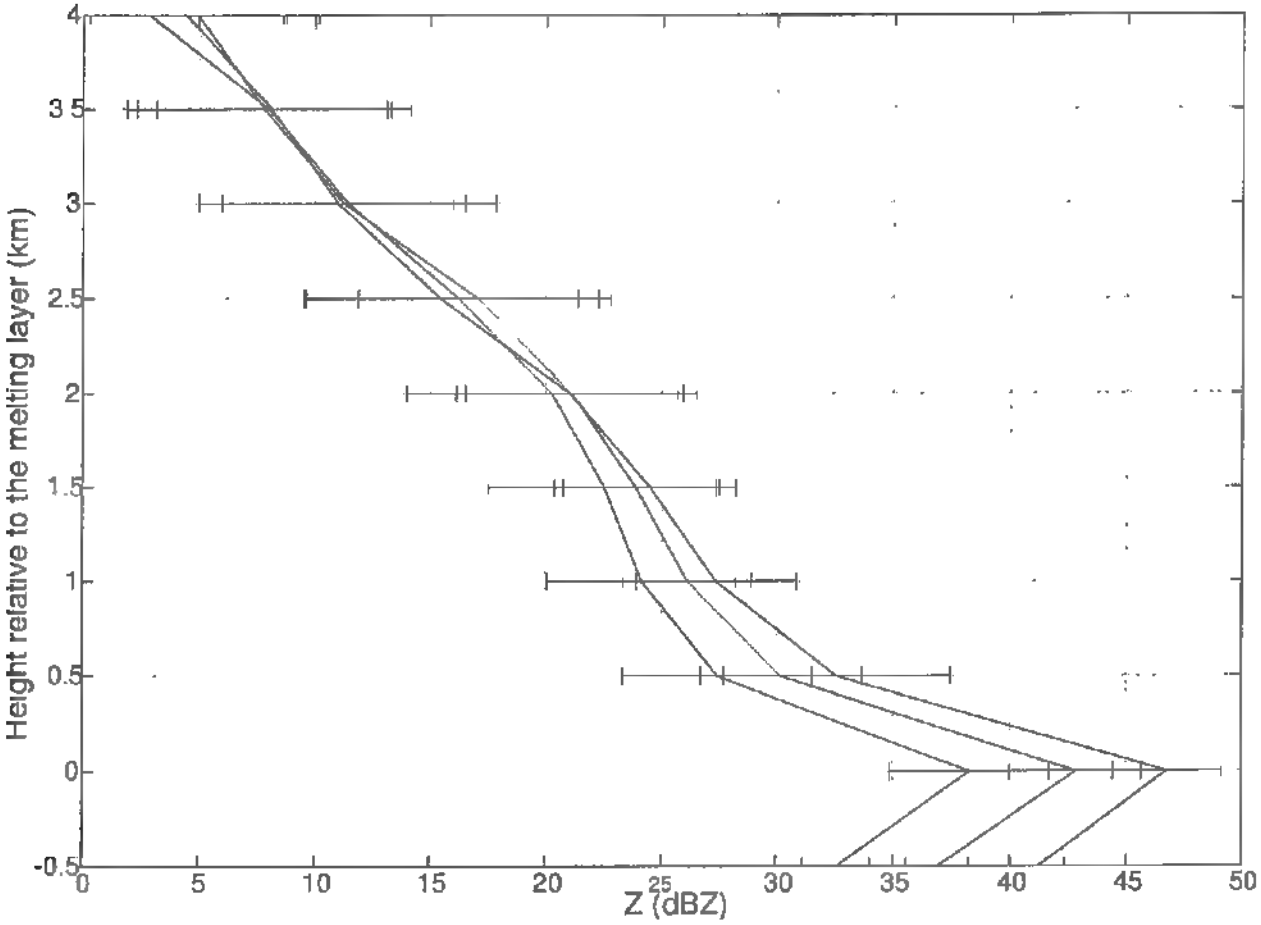
Height relative to the melting layer (km)
Z (dBZ)
4
3.5
3
2.5
2
1.5
1
0.5
0
-0.5
0
5
10
15
20
25
30
35
40
45
50

Figure 5:

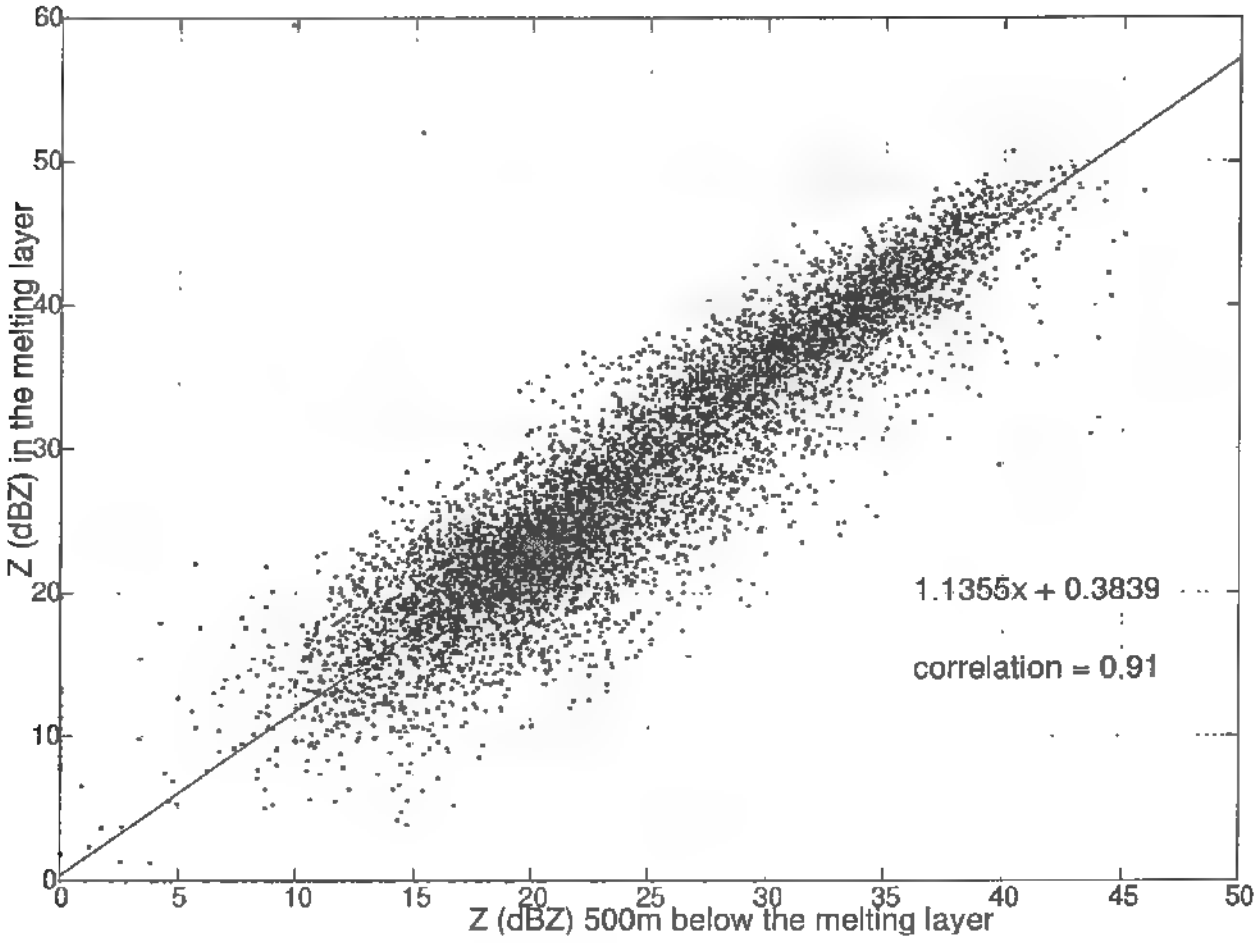
Z (dBZ) in the melting layer
Z (dBZ) 500m below the melting layer
1.1355x + 0.3839
correlation = 0.91
0
10
20
30
40
50
60
0
5
10
15
20
25
30
35
40
45
50

Figure 6:

Height relative to the melting layer (km)	α_0	α_1	correlation
0.0	1.1	0.4	0.9
0.5	0.9	-4.0	0.8
1.0	0.8	-4.0	0.7
1.5	0.8	-5.6	0.7
2.0	0.8	-7.4	0.7
2.5	0.6	-7.5	0.6
3.0	0.5	-5.0	0.5
3.5	0.3	-3.4	0.4
4.0	0.2	-2.2	0.4

Table 3:

Height relative to the melting layer (km)	graupel ±	snow ±	stratiform ±
0	3.6	5.5	3.4
0.5	5.8	5.7	4.1
1.0	7.2	5.9	4.1
1.5	8.6	5.9	5.0
2.0	9.4	5.5	6.3
2.5	10.0	5.5	6.6
3.0	10.4	4.0	6.4
3.5	10.7	4.0	6.1
4.0	11.6	3.8	5.9

Table 4:

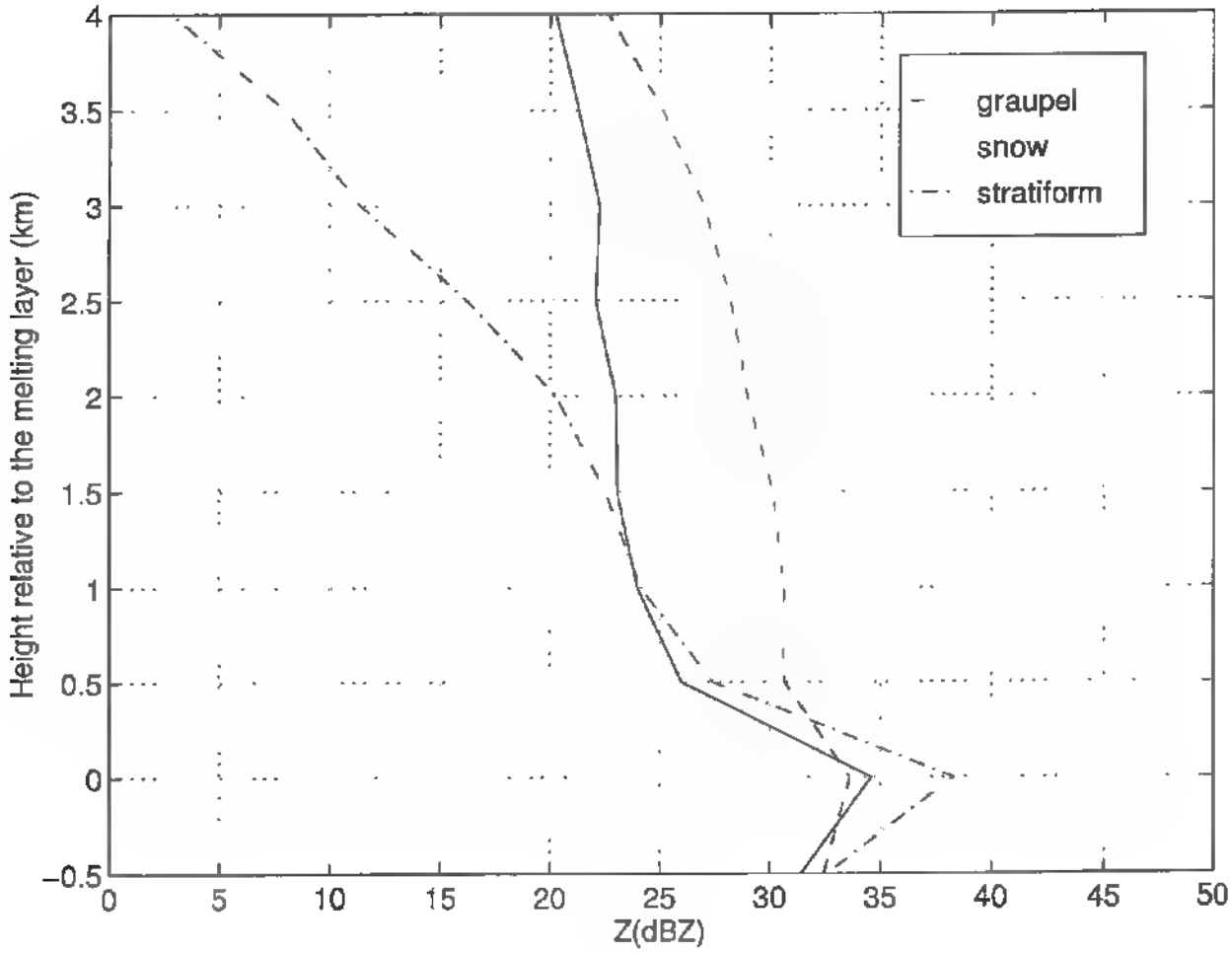
graupel
snow
stratiform
Height relative to the melting layer (km)
Z(dBZ)
4
3.5
3
2.5
2
1.5
1
0.5
0
−0.5
0
5
10
15
20
25
30
35
40
45
50

Figure 7:

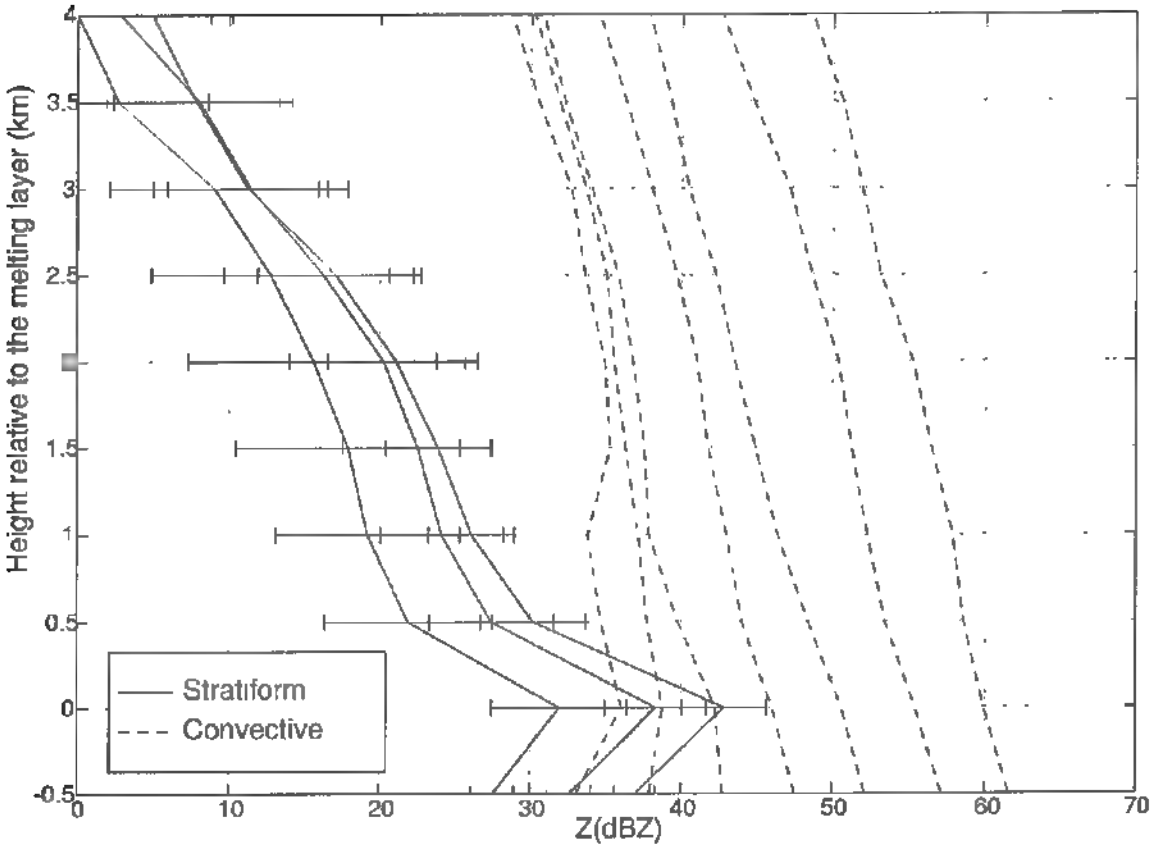

Figure 8:

Rain-bin (dBZ)	α_0	α_1	Correlation	Number of profiles
0 - 5	-0.1	0.1	0.6	22
5 - 10	0	0	NaN	90
10 - 15	-2.3	7.2	0.8	547
15 - 20	-3.6	11.7	0.9	1447
20 - 25	-5.1	17.3	0.94	1461
25 - 30	-6.3	26.6	0.98	1038
30 - 35	-6.9	32.1	0.99	1092
35 - 40	-7.4	34.4	0.99	723

Table 5:

Rain-bin (dBZ)	α_0	α_1	Correlation	Number of profiles
15 - 20	-2.5	43.6	0.7	6
20 - 25	1.3	36.4	0.6	13
25 - 30	-1.9	37.4	0.7	63
30 - 35	-1.6	36.6	0.9	232
35 - 40	-2.1	39.3	0.98	580
40 - 45	-2.4	41.1	0.98	804
45 - 50	-2.7	45.8	0.99	846
50 - 55	-3.0	49.5	1.0	625
55 - 60	-3.0	55.6	0.99	385
60 - 65	-2.9	60.6	1.0	138

Table 6:

actual(dBZ)	scheme 1. (dBZ)	scheme 2. (dBZ)	scheme 3. (dBZ)
10	8.1 ± 7.2	8.1 ± 7.2	13.0 ± 4.5
20	18.3 ± 4.4	18.5 ± 4.6	20.6 ± 3.6
30	30.2 ± 3.6	31.0 ± 4.1	30.3 ± 3.9
40	37.0 ± 3.3	41.3 ± 4.7	40.0 ± 5.3
50	43.8 ± 3.3	49.8 ± 3.9	50.0 ± 4.1
60	53.4 ± 1.9	59.9 ± 1.9	59.3 ± 1.6

Table 7:

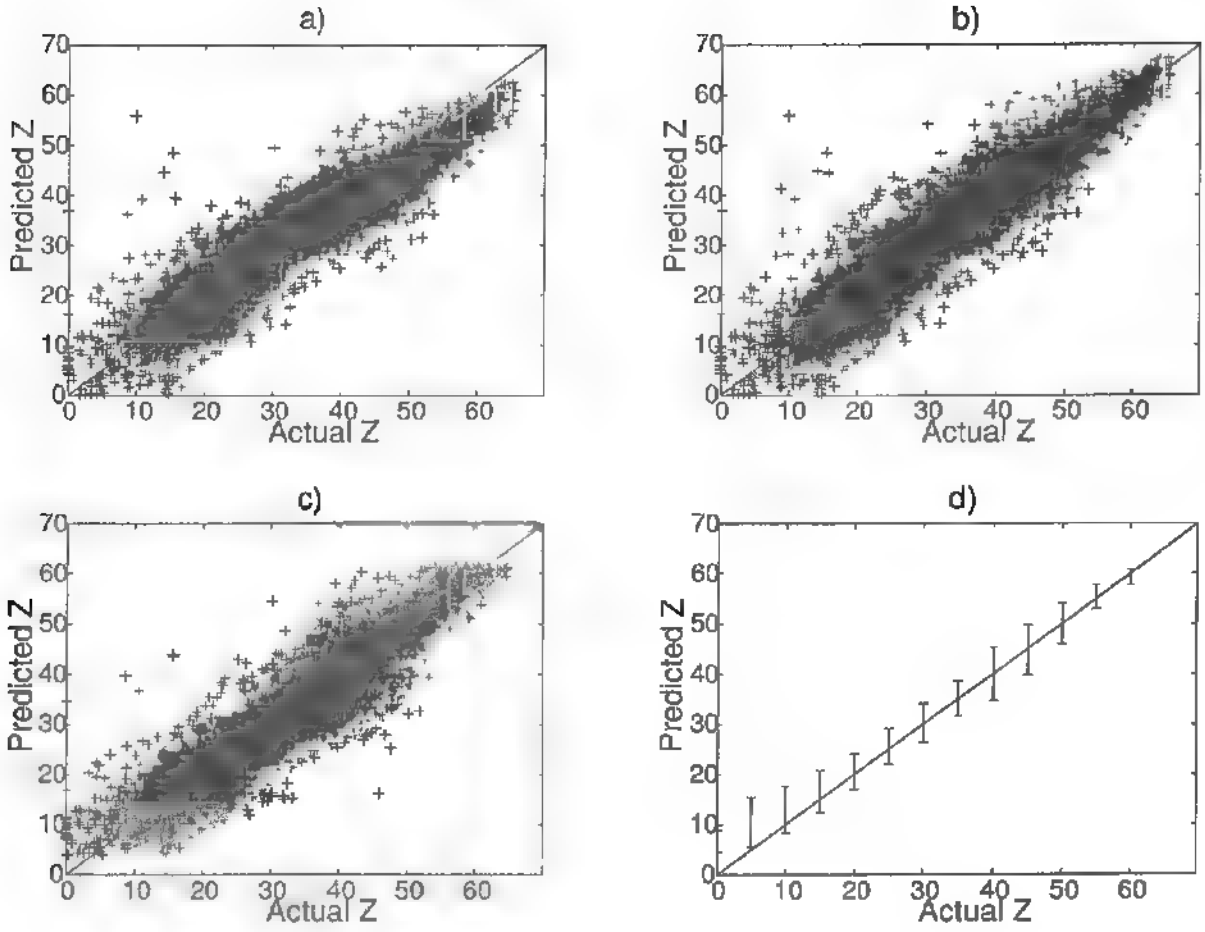

Figure 9:

CURRENT JCMM INTERNAL REPORTS

This series of JCMM Internal Reports, initiated in 1993, contains unpublished reports and also versions of articles submitted for publication. The complete set of Internal Reports is available from the National Meteorological Library on loan, if required.

1. **Research strategy and programme**
   K A Browning et al
   January 1993

2. **The GEWEX Cloud System Study (GCSS)**
   GEWEX Cloud System Science Team
   January 1993

3. **Evolution of a mesoscale upper tropospheric vorticity maximum and comma cloud from a cloud-free two dimensional potential vorticity anomaly**
   K A Browning
   January 1993

4. **The global energy and water cycle**
   K A Browning
   July 1993

5. **Structure of a midlatitude cyclone before occlusion**
   K A Browning and N Roberts
   July 1993

6. **Developments in systems and tools for weather forecasting**
   K A Browning and G Szejwach
   July 1993

7. **Diagnostic study of a narrow cold frontal rainband and severe winds associated with a stratospheric intrusion**
   K A Browning and R Reynolds
   August 1993

8. **Survey of perceived priority issues in the parametrizations of cloud-related processes in GCMs**
   K A Browning
   September 1993

9. **The effect of rain on longwave radiation**
   I Dharssi
   September 1993

10. **Cloud microphysical processes - a description of the parametrization used in the large eddy model**
    H Swann
    October 1993

11. **An appreciation of the meteorological research of Ernst Kleinschmidt**
    A J Thorpe
    May 1992

12. **Potential vorticity of flow along the Alps**
    A J Thorpe, H Volkert and Dietrich Heimann
    August 1992

13. **The representation of fronts**
    A J Thorpe
    January 1993

14. **A parametrization scheme for symmetric instability: test for an idealised flow**
C S Chan and A J Thorpe
February 1993

15. **The Fronts 92 Experiment: a Quicklook Atlas**
Edited by T D Hewson
November 1993

16. **Frontal wave stability during moist deformation frontogenesis**
Part 1: Linear wave dynamics
C H Bishop and A J Thorpe
May 1993

17. **Frontal wave stability during moist deformation frontogenesis**
Part 2. The suppression of non-linear wave development
C H Bishop and A J Thorpe
May 1993

18. **Gravity waves in sheared ducts**
S Monserrat and A J Thorpe
October 1993

19. **Potential vorticity and the electrostatics analogy: quasi-geostrophic theory**
C Bishop and A J Thorpe
November 1993

20. **Recent advances in the measurement of precipitation by radar**
A J Illingworth
April 1993

21. **Micro-physique et givrage: cloud microphysics and aircraft icing**
A J Illingworth
May 1993

22. **Differential phase measurements of precipitation**
M Blackman and A J Illingworth
May 1993

23. **Estimation of effective radius of cloud particles from the radar reflectivity**
N I Fox and A J Illingworth
May 1993

24. **A simple method of Dopplerising a pulsed magnetron radar**
A Hua, A J Illingworth and J Eastment
November 1993

25. **Radiation and polar lows**
George C Craig
February 1994

26. **Collected preprints submitted to the International Symposium on the Life Cycles of Extratropical Cyclones; Bergen, Norway, 27 June - 1 July 1994**
April 1994

27. **Convective frontogenesis**
Douglas J Parker and Alan J Thorpe
April 1994

28. **Improved measurement of the ice water content in cirrus using a total water evaporator**
Philip R A Brown and Peter N Francis
April 1994

29. **Mesoscale effects of a dry intrusion within a vigorous cyclone**
K A Browning and B W Golding
April 1994

30. **GEWEX Cloud System Study: Science Plan**
May 1994

31. **Parametrization of momentum transport by convectively generated gravity waves**
R Kershaw
May 1994

32. **Mesoscale Modelling Newsletter No 5**
May 1994

33. **Observations of the mesoscale sub-structure in the cold air of a developing frontal cyclone**
K A Browning, S A Clough, C S A Davitt, N M Roberts and T D Hewson
May 1994

34. **Longwave radiative forcing of a simulated tropical squall line**
Imtiaz Dharssi
July 1994

35. **On the nature of the convective circulation at a kata-cold front**
K A Browning
September 1994

36. **Collective preprints of papers submitted to the COST-75 International Seminar on Advanced Weather Radar Systems, Brussels, 20-23 September 1994**
November 1994

37. **Use of satellite imagery to diagnose events leading to frontal thunderstorms: Parts I and II of a case study**
K A Browning and N M Roberts
November 1994

38. **The role of spaceborne millimetre-wave radar in the global monitoring of ice cloud**
P R A Brown, A J Illingworth, A J Heymsfield, G M McFarquhar, K A Browning and M Gosset
December 1994

39. **Potential vorticity inversion**
Michal Ziemianski
October 1994

40. **Theory of mature tropical cyclones; a comparison between Kleinschmidt (1951) and Emanuel (1986)**
Suzanne L Gray
December 1994

41. **Dispersion and removal of pollutants during the passage of an atmospheric frontal system**
N R Gimson
December 1994

42. **The role of snow sublimation in frontogenesis**
D J Parker and A J Thorpe
December 1994

43. **Potential vorticity and the electrostatics analogy: Ertel-Rossby formulation**
A J Thorpe and C H Bishop
December 1994

44. **Mesoscale aspect of extratropical cyclones: an observational perspective**
K A Browning
January 1995

45. **A polar low outbreak: evolution and mesoscale structures**
T D Hewson, G C Craig and C Claud
February 1995

46. **Generation of near-surface gusts of deep convection**
K Nakamura and R Kershaw
April 1995

47. **Attribution concepts applied to the Omega Equation**
S A Clough, C S A Davitt and A J Thorpe
June 1995

48. **Parametrization of mixed-phase cloud and precipitation**
Susan P Ballard and M Gerard Hutchinson
June 1995

49. **Short-range forecasting of stratocumulus: initialization prediction**
Susan P Ballard, Simon D Jackson and B Macpherson
June 1995

50. **Contributions of the JCMM/Dept of Meteorology Radar Group to the 27th AMS Radar Meteorology Conference, Vail October 1995**
June 1995

51. **Cold pools in shear**
Douglas J Parker
September 1995

52. **High-resolution analysis of frontal fracture**
K A Browning, S P Ballard and C S A Davitt
September 1995

53. **The albedo of broken cloud fields: calculations using a modified two stream radiation code**
Imtiaz Dharssi and Roy Kershaw
October 1995

54. **Parametrization of momentum transport by convection. I: theory and cloud modelling results**
R Kershaw and D Gregory
November 1995

55. **Variation of frontal structure along a cold front**
K A Browning and N M Roberts
November 1995

56. **Secondary frontal waves**
Douglas Parker
December 1995

57. **Objective fronts**
T D Hewson
March 1996

58. **Mesoscale analysis of the activation of a cold front during cyclogenesis**
K A Browning, N M Roberts and A J Illingworth
June 1996

59. **Investigation of different representations of rain in a 1-d evaporation model**
H Swann
May 1996

60. **Parametrization of diabatic processes in the inversion of the omega-equation**
M Athanassiadou and A J Thorpe
June 1996

61. **The role of the environmental flow in the development of secondary frontal cyclones**
I A Renfrew, A J Thorpe and A Joly
June 1996

62. **Consequences of the geostrophic momentum approximation on barotropic instability**
S Malardel, A J Thorpe and A Joly
June 1996

63. **Contributions to the AMS/RMS Conference on Mesoscale Processes**
Reading, 9-13 September 1996

64. **Vorticity and potential vorticity in stratified flows interacting with an isolated obstacle**
Jorge A Gutiérrez and A J Thorpe
September 1996

65. **Triple point development: two case studies**
Douglas Parker
September 1996

66. **Radar observations of wind-shear splitting within evolving atmospheric Kelvin-Helmholtz billows**
D Chapman and K A Browning
April 1997

67. **Cold frontal structure derived from radar wind profilers**
K A Browning, D Jerrett, J Nash, T Oakley and N M Roberts
May 1997

68. **The dry intrusion and its effect on the frontal, cloud and precipitation structure of extratropical cyclones**
K A Browning - Text of invited special lecture at the Spring Conference
of the Meteorological Society of Japan, University of Tsukuba, 22 May 1997

69. **Met. Office Unified Model data, diagnostic graphics programs, and other observational data available from the JCMM through the aegis of the Universities Weather Research Network (UWERN).** (Plus supplement)
Peter Panagi and Ed Dicks
June 1997

70. **Contributions of the JCMM/Dept of Meteorology Radar Group to the 28th AMS Radar Meteorology Conference.** Austin, Texas
September 1997

71. **Sensitivity of short-range weather forecasts to local potential vorticity modifications**
Meral Demirtas and Alan Thorpe
July 1997

72. **Objective identification of frontal wave cyclones**
T D Hewson
August 1997

73. **Attribution and its application to mesoscale structure associated with tropopause folds**
A J Thorpe
September 1997

74. **The role of the environmental flow in the development of secondary frontal cyclones**
Ian A Renfrew, Alan J Thorpe and Craig H Bishop
September 1997

75. **Potential vorticity: a short history of its definitions and uses**
Alan J Thorpe and Hans Volkert
September 1997

76. **Superposing semi-geostrophic potential vorticity anomalies**
H R Birkett and A J Thorpe
September 1997

77. **Short period forecasting of catchment-scale precipitation.**
Part 1: the role of Numerical Weather Prediction
M A Pedder, M Haile and A J Thorpe
September 1997

78. **Verification of the tracking technique used in an experimental cloud motion wind inferring system**
Z Wang, K A Browning and G A Kelly
October 1997

79. **A preliminary study of Fourier series analysis for cloud tracking with GOES high temporal resolution images**
Z Wang
October 1997

80. **Analysis of an ex-tropical cyclone after reintensifying as a warm-core extratropical cyclone**
K A Browning, G Vaughan and P Panagi
November 1997

81. **A JCMM overview of FASTEX IOPs**
S A Clough, H W Lean, N M Roberts, H Birkett, J-P Chaboureau, R Dixon, M Griffiths, T D Hewson and A Montani
January 1998

82. **Programs for PV inversion and modification**
Meral Demirtas
December 1997

83. **Release of potential shearing instability in warm frontal zones**
D Chapman and K A Browning
February 1998

84. **The European Cloud-Resolving Modelling Programme (EUCREM)**
Summary Report from the coordinator
P W White
April 1998

85. **A frontal wave database**
T D Hewson
April 1998

86. **Layering observed in dropsoundings from IOP 1 of Fronts 92**
S A Clough
May 1998

87. **Use of wind-shear displays for Doppler radar data**
D Chapman and K A Browning
May 1998

88. **Radar estimates of rainfall rates at the ground in bright band and non-bright band events**
T J Smyth and A J Illingworth
June 1998

Met Office Joint Centre for Mesoscale Meteorology Department of Meteorology
University of Reading PO Box 243 Reading RG6 6BB United Kingdom
Tel: +44 (0)118 931 8425 Fax: +44 (0)118 931 8791
www.metoffice.com